ISSN 0915-633X

NATIONAL INSTITUTE FOR FUSION SCIENCE

Two- and Three-Dimensional Simulation Code for Radiation-Hydrodynamics in ICF

T. Yabe and T. Ishikawa

(Received – Oct. 16, 1991)

NIFS-119 Nov. 1991

RESEARCH REPORT
NIFS Series

NAGOYA, JAPAN

Two- and three-dimensional simulation code for radiation-hydrodynamics in ICF

T. Yabe and T.Ishikawa
Gunma University,Tenjin-chou, Kiryu, Gunma 376, Japan

Abstract

A multi-dimensional radiation hydrodynamic code is developed and is applied to the interaction of intense ion beam with plasmas. The hydrocode is based on a newly developed, highly-accurate scheme CIP (Cubic-Interpolated Pseudoparticle). The radiation transport is solved with the SSI (Symmetrical Semi-Implicit) scheme, which is quite easily implemented and is 4-5 times faster than the ICCG. The Thomas-Fermi EOS (equation of state) is used for the atomic data and the Tsakiris and Eidmann formula for the Rosseland mean-free path. This newly developed two-dimensional code is used to design an extraction method of the radiation from the high temperature regin heated by ion beam. The ion beam of 3 TW/cm^2 is converted into the soft X-ray of 40 TW/cm^2 at the surface of the radiation emitter.

Key words : Ion-beam amplification, Ion-beam-driven fusion, multi-dimensions, radiation transport, hydrodynamics

1. Introduction

We have proposed a scheme to compress and amplify an ion beam pulse[1] through soft X-ray conversion. This is so because a slowly propagating radiation wave acts as an accumulator of ion beam energy. Since the propagation speed of radiation heat wave is relatively slow, the energy flux from incident ion beam can be temporally stored within heat wave and hence the radiation power is amplified owing to this effect.

Recently, Honrubia[2] presented a calculation with a multi-group radiation transport. Although he observed a moderate power amplification, it is still not sufficient for fusion application. We can expect more effective amplification when a special configuration is used. For this purpose, we need high-speed algorithm for multidimensional hydrodynamics and radiation transport. In this paper, we propose a new and efficient algorithm and apply the method to the topic of x-ray conversion. In sections 2-4, we describe multidimensional hydrodynamic code and radiation transport code. By using this code, ion beam amplification is examined in sections 5-6.

2. Multi-Dimensional Hydrodynamic Code

Numerical methods for multi-dimensional hyperbolic equations are still a topic of considerable interest. Although many modern schemes based on an approximate Riemann solution have been proposed, they must be entirely modified in order to include various terms other than hydrodynamic processes. Adding to this, since they use a limiter function or switching function, real physical phenomena such as oscillations of high wave number are sometimes suppressed.

We have developed a new numerical method CIP (Cubic Interpolated Pseudoparticle) as a general solver for hyperbolic equations

coulpled with source, diffusion, or any other terms. This scheme has been tested with cylindrically converging shock waves, two-dimensional shock tube problem, the Rayleigh-Taylor instability, soliton formation in the KdV equation and so on. Since details are available in open literature,[3-6] we will not discuss it here. Some of the results are shown in Figs.1 and 2.

Figures 1a and 1b show the two- and three-dimensional R-T instabilities. This comparison indicates that the mushroom structure in the three dimensions is much smaller than that in two dimensions. The reason for this is attributed to the geometric nature.[6] Because of this difference in structure, the growing speed in nonlinear phase has a dependence on the geometry. This difference may cast a shadow on two-dimensional simulations frequently used, since the R-T instability is widely recognized as a source of mixing in implosion processes. The details appear in Ref.6)

These calculations are extended to the interaction of two waves in the R-T instability, where initial perturbations with two different wave numbers are imposed. The time evolution of density is given in Fig.2. This result agrees qualitatively with the result given by Anisimov[7].

3. Multi-Dimensional Radiative Heat Transfer

In simulating the ion beam amplification, we need to solve the diffusion equation :

$$\rho c_v \frac{\partial T}{\partial t} = \nabla(D \nabla T) + Q, \tag{1}$$

for radiation, where Q is the source term and/or hydrodynamic terms. In most simulation codes, a matrix solver such as the ICCG has been used. However, the ICCG is not convenient for extension to nonorthogonal grids and complex boundaries. We have proposed to

use the SSI (Symmetrical Semi-Implicit) method for this solution,[8,9] since the SSI need not use a matrix solver but is explicitly solved with a large time step.

Let us first briefly describe the basic principle of the SSI by using a linear diffusion equation :

$$\frac{\partial T}{\partial t} = \nabla^2 T, \tag{2}$$

In the semi-implicit scheme, Eq.(2) is put into a finite difference form

$$\frac{T_i^{n+1} - T_i^n}{\Delta t} = \frac{T_{i+1}^n - 2T_i^{n+1} + T_{i-1}^n}{\Delta x^2}, \tag{3}$$

This scheme is unconditionally stable. This can be illustrated as follows. If $\Delta t \to \infty$, then Eq.(3) gives simply $T_i^{n+1} = (T_{i+1}^n + T_{n-1}^n)/2$. As easily understood, the profile at $n+2$ is the same as that at n. Therefore, the small scale perturbation given at n will not be amplified.

Although the scheme is stable, however, answer given by Eq.(3) is comletely wrong. In order to show this, let us write down finite difference forms on the neighbouring points.

$$T_i^{n+1} - T_i^n = \frac{\Delta t}{\Delta x^2}[(T_{i+1}^n - T_i^{n+1}) - (T_i^{n+1} - T_{i-1}^n)], \tag{4}$$

$$T_{i+1}^{n+1} - T_{i+1}^n = \frac{\Delta t}{\Delta x^2}[(T_{i+2}^n - T_{i+1}^{n+1}) - (T_{i+1}^{n+1} - T_i^n)], \tag{5}$$

The first half $(T_{i+1}^n - T_i^{n+1})$ on the right-hand side (r.h.s.) of Eq.(4) is the flux transported from the grid $i+1$ and hence should be the same as the second half $(T_{i+1}^{n+1} - T_i^n)$ on the r.h.s. of Eq.(5). Unfortunately, however, these two fluxes are not the same, because of the difference of the superscript n. Therefore, $\delta_{i+1/2}^{n+1} = (T_{i+1}^n - T_i^{n+1}) - (T_{i+1}^{n+1} - T_i^n)$ flows into the system. The error should be

subtracted from the system. In the SSI, $-\delta^{n+1}_{i+1/2}\Delta t/2\Delta x^2$ is added to both Eqs.(4) and (5). It is illustrating to rewrite this δ^{n+1} as $\delta^{n+1}_{i+1/2} = (T_{i+1}+T_i)^n - (T_{i+1}+T_i)^{n+1}$. This means the error depends on the time evolution of the average temperature at $i+1/2$. In some cases, this error correction may procced further to accelerate the change. In reality, if we make the correction after T^{n+1} is obtained such as $T^{n+1} = T^{n+1} - \delta^{n+1}\Delta t/2\Delta x^2$, this leads to an instability, especially when the heat is input from outside.

It is important to know that the solution of Eq.(3) is given by

$$T^{n+1}_i = \frac{(T^n_{i+1} + T^n_{i-1} + \alpha)(\Delta t/\Delta x^2)}{1 + \Delta t/\Delta x^2}. \tag{6}$$

If we can add the correction δ on the r.h.s. of Eq.(3), then $\alpha = -(\delta^{n+1}_{i+1/2} + \delta^{n+1}_{i-1/2})\Delta t/2\Delta x^2$ and the temperature change given by Eq.(6) is not simply proportional to δ but to $\delta/(1 + \Delta t/\Delta x^2)$. If $\Delta t/\Delta x^2$ becomes quite large, this way of correction guarantees the stability because of the reduction of feedback by a factor of $1/(1 + \Delta t/\Delta x^2)$. It is not possible to add the correction at $n+1$ to Eq.(6) because T^{n+1} is not yet calculated. Therefore, the SSI proposes to add the correction with the time lag, that is , $\alpha = -(\delta^n_{i+1/2} + \delta^n_{i-1/2})(\Delta t)^{old}/2\Delta x^2$. The superscript "old" in Δt means the time increment at n-th step. This time lag can also cause the time lag of the energy conservation, which means that the energy from the error correction is not correctly added to the current time step although the error does not accumulate in time. In the case shown later, this error is only a few percent even for $D\Delta t/\Delta x^2 \sim 1000$.

Here, we present a benchmark test for the SSI. Figure 3 shows the time evolution of radiation wave. 20 x 20 grids are used with $\Delta x = \Delta y = 1$. Initially, $T = 1.0$ for $8 \leq i \leq 12$ and $8 \leq j \leq 12$ and $T = 0.01$ for the other region. Top and bottom figures, respectively, show the results with the SSI and ICCG. Here, the time step is

controlled by

$$\Delta t^{new} = \epsilon \times \Delta t^{old} \frac{T^{n+1} + T^n}{T^{n+1} - T^n}, \tag{7}$$

$$0.5\Delta t^{old} \leq \Delta t^{new} \leq 1.2\Delta t^{old}, \tag{8}$$

where $\epsilon = 0.4$ in Fig.3. Equation (8) is used in order to avoid an abrupt change of Δt in time. Initially, the time step is set to be quite small ($\Delta t = 0.01$) and then becomes larger later on. In Fig.4, normalized time step ($\Delta t/\Delta x^2$) is plotted versus time step. In these tests, the computation time required by the SSI is 4-5 times shorter than that by the ICCG.

Since the original SSI[8] is given only for one-dimensional case, it is of use to show its three-dimensional finite difference form of Eq.(1).

$$T^{n+1}_{i,j,k} = (Q^n_{i,j,k} + \rho c_v T^n_{i,j,k}/\Delta t + B1 + B2 + B3)/B4$$

where $B1 - B4$ are defined as

$$B1 = [D_{i+1/2,j,k}T^n_{i+1,j,k} + D_{i-1/2,j,k}T^n_{i-1,j,k} + (\delta^x_{i+1/2,j,k} + \delta^x_{i-1/2,j,k})/2]/\Delta x^2$$
$$B2 = [D_{i,j+1/2,k}T^n_{i,j+1,k} + D_{i,j-1/2,k}T^n_{i,j-1,k} + (\delta^y_{i,j+1/2,k} + \delta^y_{i,j-1/2,k})/2]/\Delta y^2$$
$$B3 = [D_{i,j,k+1/2}T^n_{i,j,k+1} + D_{i,j,k-1/2}T^n_{i,j,k-1} + (\delta^z_{i,j,k+1/2} + \delta^z_{i,j,k-1/2})/2]/\Delta z^2$$
$$B4 = \rho c_v/\Delta t + (D_{i+1/2,j,k} + D_{i-1/2,j,k})/\Delta x^2 + (D_{i,j+1/2,k} + D_{i,j-1/2,k})/\Delta y^2 + (D_{i,j,k+1/2} + D_{i,j,k-1/2})/\Delta z^2,$$

where

$$\delta^x_{i+1/2,j,k} = DO_{i+1/2,j,k}[(T^n_{i+1,j,k} + T^n_{i,j,k}) - (T^{n-1}_{i+1,j,k} + T^{n-1}_{i,j,k})]$$

$$\delta^y_{i,j+1/2,k} = DO_{i,j+1/2,k}[(T^n_{i,j+1,k} + T^n_{i,j,k}) - (T^{n-1}_{i,j+1,k} + T^{n-1}_{i,j,k})]$$

$$\delta^z_{i,j,k+1/2} = DO_{i,j,k+1/2}[(T^n_{i,j,k+1} + T^n_{i,j,k}) - (T^{n-1}_{i,j,k+1} + T^{n-1}_{i,j,k})]$$

We have introduced $D_{i+1/2,j}$, which is calculated by $T_{i+1/2,j,k} = (T_{i+1,j,k} + T_{i,j,k})/2$ and $\rho_{i+1/2,j,k} = (\rho_{i+1,j,k} + \rho_{i,j,k})/2$, and similar definition is used for the subscripts j and k. D is given at the time step n. DO means D at the previous time step multiplied by $\Delta t^{old}/\Delta t$, Δt^{old} being the time increment at the previous time step.

4. Atomic Model and Beam-Energy Deposition

There have been a strong interest in the non-LTE (Local Thermodynamic Equilibrium) atomic model, because of high rate of radiation from high-Z material. In these plasmas, the non-LTE is a key issue in determining the radiation flux from the surface irradiated by intense laser light. However, the calculation time required for this process becomes a large fraction of complete calculation. This gives a serious constraint in extending the code to multi-dimensions. We use , instead, the Thomas-Fermi atomic model because most parameter regime in ion-beam-driven fusion is in LTE.

The specific heat c_v in the T-F approximation is given by Latter[10] and put into a formula by Bell[11]. The program list is given in Fig.5. The average charge state is used in the ion-beam stopping power, whose program list is given in Fig.6 according to Mehlhorn's paper[12]. The result with the T-F model is calculated by More[13] and is put into a convenient form. The result is also given in Fig.5.

The diffusion coefficient D for the radiation in Eq.(1) is given by

$$D = \frac{16\sigma\lambda_R T^3}{3}, \tag{9}$$

where $\sigma(= 5.6705 \times 10^{-5}$ erg/cm^2·sec·deg^4) is the Stefan-Boltzmann constant. λ_R is the Rosseland mean free path and its approximate formula is given by Tsakiris and Eidmann[14]. Here, we repeat the

formula

$$\frac{1}{\rho\lambda_R} = aT^s\rho^r \tag{10}$$

where the values of a, s, r are given in Ref.14).

5. Analysis of Ion Beam Amplification

If the ion beam is incident on high-Z material that is optically thick, the energy propagates through it like a diffusion wave. In the diffusion process, the size of a heated region expands in proportion to $t^{1/2}$, while the ion beam energy is injected in proportion to t. Thus, the energy is accumulated in this region causing high temperature. Since the radiation power is proportional to σT^4, small increase of temperature largely enhances the radiation power.

The equation for the propagation of radiation is given by Eqs.(1) and (9) for nearly equilibrium situation. If we estimate the propagation length L of the radiation wave within a time t such as $\partial T/\partial t \sim T/t$ and $\nabla T \sim T/L$, then we have $L = [(16\sigma\lambda_R T^3 t)/(\rho c_v)]^{1/2}$ from Eqs.(1) and (9). The thermal energy accumulated in this region L is $\epsilon = \rho c_v T L$ and this energy must be supplied from the ion beam It. This balance determines the evolution of temperature. The black body radiation flux σT^4 from this plasma is given by[1,15)]

$$\frac{\sigma T^4}{I} = \frac{3L}{16\lambda_R}. \tag{11}$$

or in an explicit form

$$T^4 = (\frac{9}{16}\frac{I^2 t\rho^r a}{\sigma c_v})^{4/(5-s)}. \tag{12}$$

Equation (12) suggests the converter material having larger a and smaller s. Therefore, we will use gold as a converter in the simulation given in the next section. The above relation implies that the

radiation intensity can be larger than the incident ion beam intensity if the length of amplifier is sufficiently longer than the radiation mean free path. Equation (11) also raises another problem on how to extract the radiation energy from such an optically thick plasma. In some case, the amplifier and the target may be the same[1] or fused shutter[2] may be neccesary. In the next section, we will discuss this point more clearly.

The above-mentioned scaling has been investigated in detail[1] using the one-dimensional hydrocode HIMICO coupled with average ion model and multi-group radiation transport as well as the ion beam stopping calculation similar to that given by Mehlhorn.[12] In the next section, we will show one- and two-dimensional simulations but with a simplified physics included as stated in sections 2-4.

6. Simulation of Ion Beam Amplification

The important point in ion-beam-driven fusion is how to use the radiation from the region of the highest temperature. When the ion beam is injected from the righthand side and the radiation wave propagates leftward, the temperature decreases to the left. This decrease is not much for the radiation because of large nonlinearity of the diffusion coefficient. However, since the radiation power is proportional to σT^4, it is sensitive to this decrease. Therefore, it is important to find a way to extract the radiation from high temperature region. In this section, we propose some possible methods to do this.

In the simulation shown in Fig.7, the two proton beams are incident from both sides, where the proton beam is 1.5 MeV, 3TW/cm^2 at peak, which is triangular in time and linearly rises in time until 30 ns and decreases linearly until 60 ns. The material of the x-ray converter is a low-density gold of 0.1 g/cm^2. The figure shows the

time evolution of the temperature profile for every 2 ns up to 80 ns.

Four different cases are compared. In Fig.7a, 7b, 7c, two sides are open for radiation to escape, whereas two-sided boundaries are mirror in Fig.7d. Only one beam is incident in Fig.7a and two beams are incident in other figures. In Fig.7c high-density gold layer is placed outside the converter, where the ion beam is put into only the converter passing through this high-density tamper. In any case except for Fig.7a, however, the temperature at the center behaves very similarly. This means the effect of radiation escape is quite small in these configuration as already pointed out by our previous papers[1]. By changing the length of layer, we compared the maximum temperature up to 80 ns obtained for 4 different configurations and show it in Fig.7.

It is surprising that a peak temperature of $\sim$ 160 eV is attained even with such a low intensity beam. The flux of the thermal radiation corresponding to 160 eV is 67 TW/cm^2. In Fig.7c, we can use a special configuration for the beam to pass through a high-density gold layer. For example, magnetic fields can be used to pinch the beam at a hole placed on the high-density gold layer. After passing this hole, the beam may expands and illuminates the converter with a wide and low intensity. It is of use to note, however, even in the open geometry like in Fig.7b, sufficiently high temperature can be attained.

It seems curious that the temperature increase with two colliding beam is not twice as large as that with one beam. Since the ion beam stopping length becomes shorter when the temperature increases, two ion beams do not overlap with each other in later phase and therefore the situation becomes quite similar to one-sided beam.

One possibility to extract this radiation is to use a configuration shown in Fig.9. The radiation waves propagate through the tube and collide in the middle of the tube, where the radiation is extracted in

a perpendicular direction through a hole on the wall of the tube.

Another method is to use the focusing of the radiation. Since the propagation speed of the radiation is inversely proportional to the density, the radiation wave directs towards the high-density region. By properly changing the gold gas density, the two radiation waves can collide at any place we like. Variable-density foam layers of this kind have already been demonstrated by the target fabrication group at ILE, Osaka University. Figure 10 shows the configuration used in the simulation, whose results are shown in Fig.11. Here, the increment of the contour is 5 eV. The gold density linearly varies from 0.05 g/cm^3 (top) to 0.15 g/cm^3 (center). Since the ion beam stopping length is also inversely proportional to the density, the radiation wave is driven obliquely from the begining.

The radiation wave should be designed to collide at the inner surface of the amplifier which is the outer surface of the target placed at the center, where we placed a solid gold sphere in the present calculation. Although the calculation shown in Fig.11 is not yet optimized, the temperature of 140 eV at this surface is already attained. The radiation from plasmas of 140 eV is about 40 TW/cm^2. Therefore, the intensity of incident ion beam is amplified by more than 10 times even in this low intensity beam of 3 TW/cm^2.

7. Summary

We have developed a new two-dimensional hydrodynamic code including radiation transport which is solved with the SSI method with high efficiency. Implementatin of this code is quite easy compared with the preceding schemes. This code is applied to the ion beam amplification. A new extraction method of the radiation from the region of the highest temperature has been proposed and more than 10 times amplification has been demonstrated even in the case

of 3 TW/cm^2 ion beam, which is available at present and is a parameter close to PBFA II at SNL. The amplification will increase in proportion to the incident power.

The important point in this paper is that the amplification of the power is of no doubt but the radiation power which can be effectively used depends on the extraction method. For the latter, there may be a variety of schemes. We have proposed only two schemes. In such a design, two and three dimensional code is quite effective. More effective schemes are under consideration.

Acknowledgements

This work was carried out under the collaborating research program at the National Institute for Fusion Science. One of the authors (T.Y.) would like to thank Professor Dr. F. Winterberg for indicating a possibility of focusing radiation heat waves through variable density and thank Dr. B.Goel and Dr. J.J.Honrubia for valuable discussion.

References

1) T.Yabe, Jpn.J.Appl.Phys. **23**(1984)L57, **24**(1985)L104, **26** (1987)L296.
2) J.J.Honrubia, Laser and Particle Beams **8** (1990)117.
3) H.Takewaki, T.Yabe. J.Comput. Phys. **70**, 355 (1987).
4) T.Yabe and E.Takei, J.Phys.Soc.Japan **57** (1988) 2598.
5) T.Yabe *et al.*, Comput. Phys. Comm. **66** (1991) 219 and 233..
6) T.Yabe, H.Hoshino and T.Tsuchiya, Phys. Rev. **A** (1991)
7) S.I.Anisimov, private communication.
8) E.Livne and A.Glasner, J.Comput. Phys. **58** (1985) 59.

9) T.Ishikawa and T.Yabe, The Fourth IEEE Conference on Electromagnetic Field Computation, Tronto, Ontario, October (1990).
10) R.Latter, Phys. Rev. **99** (1955) 1854.
11) A.R.Bell, *New Equation of State for MEDUSA*, Rutherford Laboratory Report, RL-80-091 (1981).
12) T.A.Mehlhorn, J. Appl. Phys. **52** (1981) 6522.
13) R.M.More, *Atomic Physics in Inertial Confinement Fusion*, UCRL-84991 Part I and II. (1981).
14) G.D.Tsakiris and K.Eidmann, J.Quant.Spectrosc.Radiat. Transfer **38** (1987) 353.
15) K.Unterseer and J.Meyer-ter-Vehn, Jpn.J. Appl. Phys. **23** (1984) L728.

Figure Captions

Fig.1: Density contours in the R-T instability at $t = 0.51$ when $g = 1.0$. Initial velocity perturbation V is 0.8. (a)-(c) Two-dimensional results. (d)-(f) Three-dimensional results. The mesh size is $\Delta x = \Delta y = 0.01(60 \times 30)$ in (a), $\Delta x = \Delta y = 0.01/2(120 \times 60)$ in (b), $\Delta x = \Delta y = 0.01/3(180 \times 90)$ in (c), $\Delta x = 0.01$ and $\Delta y = \Delta z = 0.01 \times 2^{1/2}(60 \times 30 \times 30)$ in (d),$\Delta x = 0.01/2$ and $\Delta y = \Delta z = 0.01/2 \times 2^{1/2}(120 \times 60 \times 60)$ in (e),$\Delta x = 0.01/3$ and $\Delta y = \Delta z = 0.01/3 \times 2^{1/2}(180 \times 90 \times 90)$ in (f).

Fig.2: The same run as the two-dimensional case in Fig.1 but with two different initial perturbations.

Fig.3: Time evolution of radiation wave. (Top) SSI, (Bottom) ICCG. The profiles of every time step are shown.

Fig.4: Change of normalized time step ($D\Delta t/\Delta x^2$, $D = 1$ in this example) used in the calculation of Fig.3.

Fig.5: Program list of the Thomas-Fermi EOS.

Fig.6: Program list of ion beam stopping.

Fig.7: One-dimensional simulation of ion-beam-energy conversion into X-ray. (a) One beam, open boundary, (b) Two beams, open boundary, (c) Two beams, with tamper, (d) Two beams, mirror boundary.

Fig.8: Maximum temperature up to 80 ns in Fig.7. Closed circles, open squares, closed squares and open circles correspond to Figs.7a, 7b, 7c and 7d, respectively.

Fig.9: If the tube has a hole in the middle, radiation from the colliding thermal waves can be extracted.

Fig.10: Alternative scheme with uses the focusing of thermal waves. Density changes vertically but not horizontally. This density change has already been demonstrated by ILE target group at Osaka University using foam layered target.

Fig.11: Time evolution of temperature in the amplifier proposed in Fig. 10. Time proceeds from top to bottom as 30, 40, 50, 60 nsec. The increment of the contour is 5 eV.

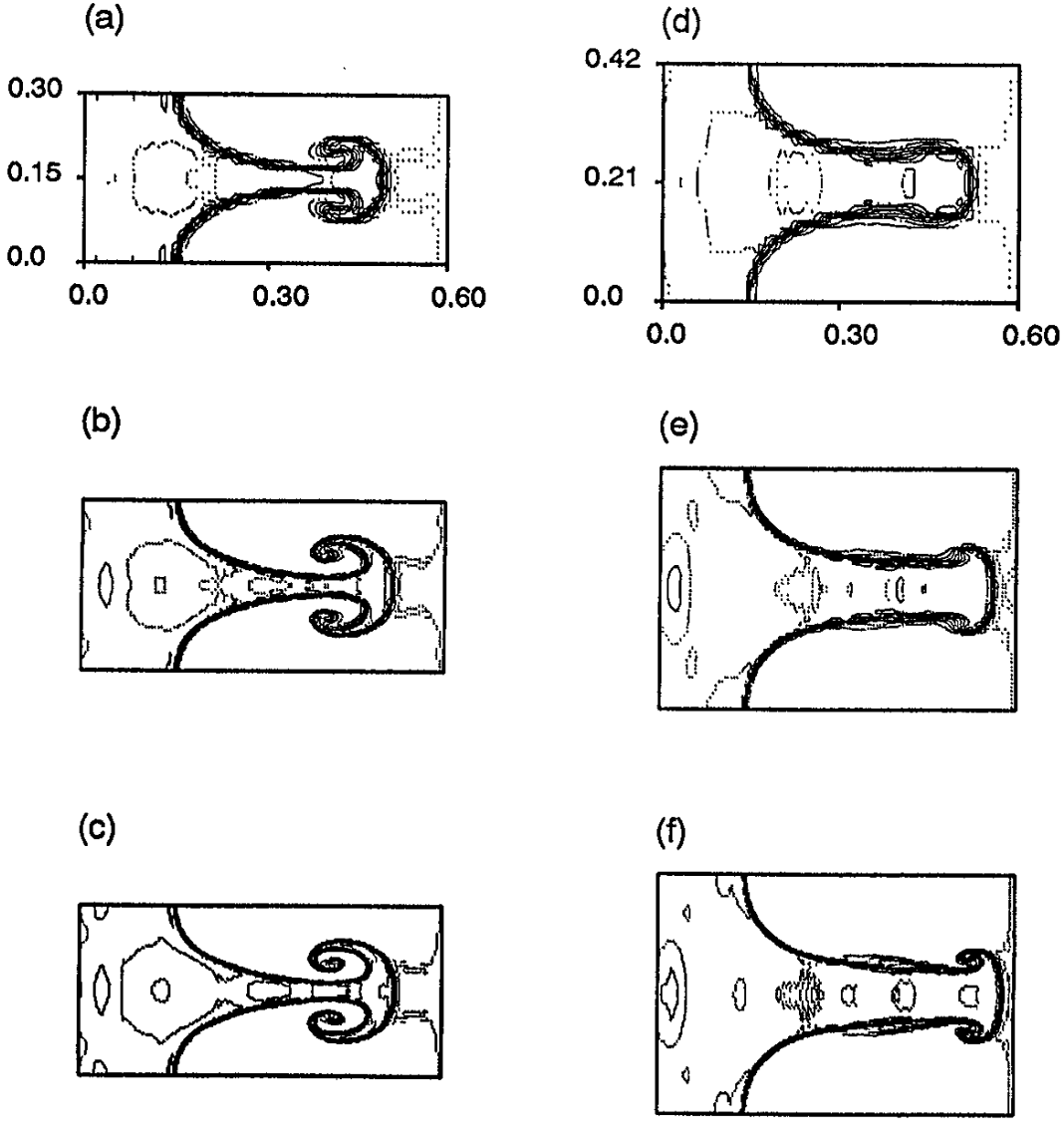

Fig.1

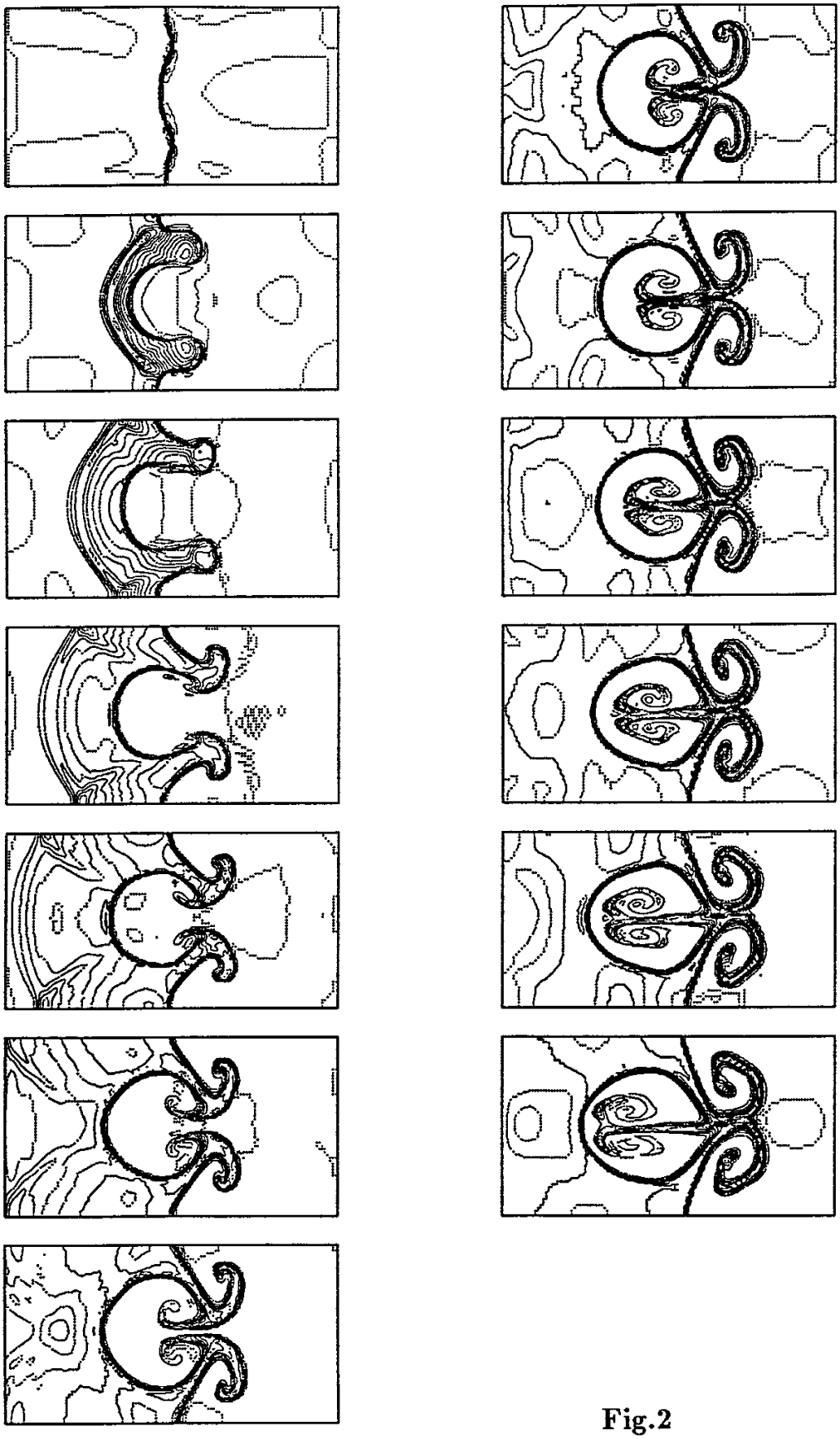

Fig.2

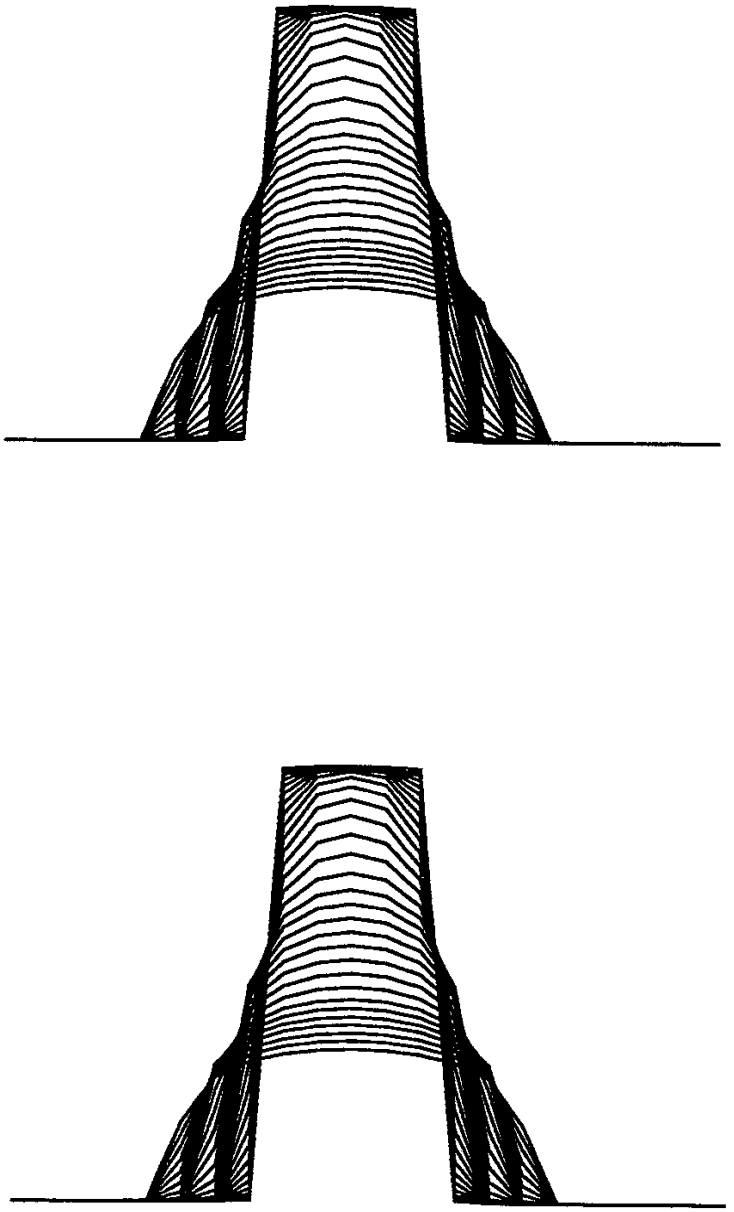

Fig.3

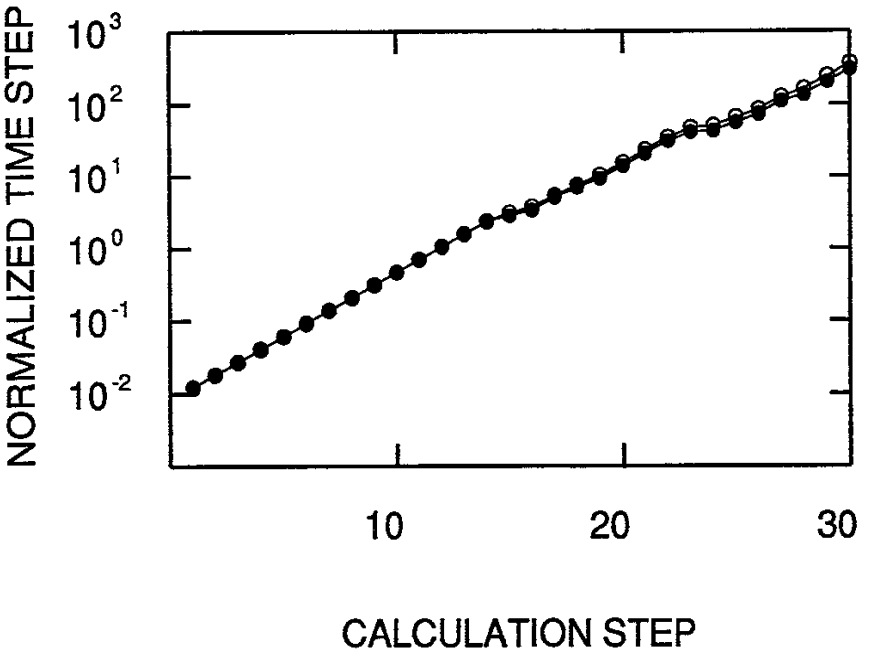
NORMALIZED TIME STEP
10^3
10^2
10^1
10^0
10^{-1}
10^{-2}
10
20
30
CALCULATION STEP

Fig.4

```
C*************************************************************************
C*     THOMAS-FERMI EOS
C*        YT --- TEMPRETURE (eV)    YR --- DENSITY (g/cm^3)
C*        Z0 --- ATMIC NUMBER       AM --- ATOMIC MASS
C*************************************************************************
         A( 1 ) = 4.486D+10
         A( 2 ) = 0.0
         A( 3 ) = 8.5383D+17
         A( 4 ) = 1.3811D+21
         A( 5 ) = 5.5707D+24
         A( 6 ) = 1.585D-12
         A( 7 ) = 6.760D-13
         A( 8 ) = 3.333D+9
         A( 9 ) = 7.627D+20
         A( 10 ) = 13.172
         A( 11 ) = 1.7562
         A( 12 ) = 3.283D+7
         A( 13 ) = 1.805D+8
           ZTFT0 = YT(I,J,K)/ Z0(I,J,K)**1.33333D0
           ZTFR  = YR(I,J,K)/AM(I,J,K)/ Z0(I,J,K)
           ZTFTF = ZTFT0 / ( 1.0D0 + ZTFT0 )
           ZTFA = 0.003323D0 * ZTFT0 ** 0.971832D0
     &          + 9.26148D-5 * ZTFT0 ** 3.10165D0
           ZTFB = - DEXP( - 1.7630D0 +1.43175D0*ZTFTF
     &          +0.315463D0*ZTFTF **7 )
           ZTFC = - 0.366667D0 * ZTFTF + 0.983333
           ZTFQ1 = ZTFA * ZTFR ** ZTFB
           ZTFI = 1.D0 / ZTFC
           ZTFQ  = ( ZTFR **ZTFC + ZTFQ1 ** ZTFC ) ** ZTFI
           ZTFX  = 14.3139 * ZTFQ ** 0.6624D0
C
C<<<<<< THOMAS-FERMI EFFECTIVE CHARGE >>>>>>
           ZZ(I,J,K) = Z0(I,J,K)*ZTFX/(1.D0+ZTFX+DSQRT(1.D0+2.D0*ZTFX))
C
           ZT = YT(I,J,K)/Z0(I,J,K)**(4./3.)
           ZV = Z0(I,J,K)*AM(I,J,K)*1.673E-24/YR(I,J,K)
           P1 = 1.602D-12*ZT/ZV
           P2 = 0.0D0
             DO 100 N = 1 , 5
               Z110 = FLOAT( N ) / 6.0 + 0.5
 100           P2 = P2 + A(N)*ZV**Z110
           P2 = P2 ** (-2.5)
           P4 = A(6) * ZT
           P5 = A(7) * ZT ** 1.61
           P3 = ( 1.D0/ZV - 0.75D-18*ZV**(-1.75) )
     &          *( P4**(-2.0) + P5**(-2.0) ) ** (-0.5)
     &          + 0.75D-18*ZV**(-1.75)*P5
C
C<<<<<< THOMAS-FERMI PRESSURE (IN CGS UNIT) >>>>>>
           PRE(I,J) = ( 0.2*P1 + P2 +0.8*P3 ) * Z0(I,J)**(10./3.)
C
           DUT1 = 1.5
           DUT3 = ( 1.D-18*ZV**(-0.75) + DLOG(ZV*1.D22) )
     &           *( 1.61*A(13)*ZT**(-2.0733333)
     &            - 0.22*A(12)*ZT**(-0.853333) )
     &           *( A(12)*ZT**0.146666 + A(13)*ZT**(-1.073333) )**(-2.5)
           DUT4 = 1.5*ZT*( 2.2 + ZT )*( 1.1 + ZT ) ** (-2.0)
C
C<<<<<< THOMAS-FERMI SPECIFIC HEAT C_v*m_i/k_B=CVE >>>>>>
           CVE(I,J,K) = ( 0.2*DUT1 + 0.8*( DUT3+DUT4 ) ) * Z0(I,J,K)
```

Fig.5

```
C*********************************************************************
C*     ION BEAM STOPPING BY MEHLHORN                                 *
C*********************************************************************
      DATA  ( ZSCA( I ) , I = 1 , 5 ) /-17.02,5.846,-0.7149
     &       ,0.0374,-0.0007114/
        EEB=1.5                 : (BEAM ENERGY IN MEV)
        ZBEAM=1.0               : (BEAM ATOMIC NUMBER)
        ABEAM=1.0               : (BEAM MASS NUMBER)
        PE0=3.0                 : (BEAM POWER IN TW)
        C0  = 3.E10
        Z5  = 0.307
        Z6  = 0.764 * C0 / 5.64E4
        Z7  = 1.022E6
        Z20 = 1.E19
        TPULS=30.E-9            : (BEAM PULSE WIDTH IN SEC)
        FPP = T / TPULS         : (T IS TIME IN SEC)
        IF( T . GT . TPULS ) FPP = 1. - ( T - TPULS ) / TPULS
        IF( T . GT . TPULS ) FPP = 1.
        EEBP = EEB
        ZPE = Z20 * PE0 / EEBP * FPP
C
C****** ZERO CLEAR HEAT(I,J,K) = HEATING ENERGY IN ERG/CC
C
      DO 1000 K=1,NZ            : NX,NY,NZ=MESH NUMBER IN X,Y,Z
      DO 1000 J=1,NY
C
      DO 30 I = 1 , NX
        EEHB( I ) = 0.0         : (BEAM ENERGY -- CHANGE AFTER DEPOSITION)
        SPW( I )  = 0.0         : (STOPPING POWER)
   30 C O N T I N U E
        EEHB( NX ) = EEBP
C
        DO 10 I = 1 , NX - 1
        L = NX - I
C>>>
C>>>------- ZBETA = V/C , ZOMEG = PLASMA FREQ.              ------<<<
C>>>------- EEHB = ION ENERGY (MEV), ZBMIN = IMPACT PARAM. ------<<<
C>>>------- ZZ = ZEFF OF TARGET, ZEFBM= ZEFF OF BEAM       ------<<<
C>>>
        ZBETA = SQRT( EEHB( L + 1 ) / ( 4.691E2 * ABEAM ) )
        ZBETS = ZBETA * ZBETA
        YDEN=YR(L,J,K)/(AM(I,J,K)*1.673E-24)
        ZOMEG = SQRT( ZZ(I,J,K)*YDEN)
        ZEFBM = ZBEAM * ( 1.0 - 1.034
     &            * EXP( -137.0 * ZBETA / ZBEAM ** 0.69 ) )
        ZBMIN = AMAX1( 2.8179E-13 * ZEFBM / ZBETS ,
     &           3.8616E-11 / ZBETA )
C>>>
C>>>------- STOPPING POWER (FREE ELECTRON)  MEV/GCM2        ------<<<
C>>>
       ZSTPFR = Z5 * ZEFBM * ZEFBM * ZZ(I,J,K)
     &        * ALOG( Z6 * ZBETA / ( ZOMEG * ZBMIN ) )
     &        / ( ZBETS * AM(I,J,K) )
C>>>
C>>>------- STOPPING POWER (BETHE FORMULA)  MEV/GCM2        ------<<<
C>>>------- Z0 = ATOMIC NUMBER OF TARGET                    ------<<<
C>>>
        ZI1 = 13.6 * ZZ(I,J,K) * ZZ(I,J,K)
        ZI2 = 9.0 * Z0(I,J,K) * ( 1.0 + 1.8 / Z0(I,J,K) ** 0.666666 )
        ZI0 = AMAX1( ZI1 , ZI2 )
CX      ZLI = DLOG( ZI0 )
        Z10 = Z7 * ZBETS / ( ( 1.0 - ZBETS ) * ZI0 )
C>>>
C>>>------- SHELL CORRECTION                                ------<<<
C>>>
        ZEAMU = EEHB( L + 1) * 1.E+3 / ABEAM
        ZELG  = ALOG( ZEAMU )
        ZMULT = 1.0 / ZELG
        ZSHLL = 0.0
          DO 100 KK = 1 , 5
            ZMULT = ZMULT * ZELG
            ZSHLL = ZSHLL + ZSCA( KK ) * ZMULT
  100     C O N T I N U E
        Z10 = ALOG( Z10 ) - ZBETS - ZSHLL
        IF( Z10 . LE . 0.0 ) Z10 = 0.0
C
      ZSTPBT = Z5 * ZEFBM * ZEFBM * ( Z0(I,J,K) - ZZ(I,J,K) ) * Z10
     &       / ( ZBETS * AM(I,J,K) )
C>>>
C>>>------- STOPPING POWER (LSS FORMULA ) MEV/GCM2          ------<<<
C>>>
        ZATL0 = ZBEAM ** 0.666667 + Z0(I,J,K) ** 0.6666667
        ZATL  = 1.0 / SQRT( ZATL0 )
        ZRA   = AM(I,J,K) / ABEAM
        ZK    = 0.0793 * ZBEAM ** 0.666667 * SQRT( Z0(I,J,K)
     &          / AM(I,J,K) ) * ( 1.0 + ZRA ) ** 1.5
     &          / ZATL0 ** 0.75
       ZSTPLS = 9.129E5 * ZK * SQRT( ( 1.0 + ZRA ) * ZBEAM * Z0(I,J,K)
     &          / ( ZRA * ZATL ) * EEHB( L + 1 ) )
     &          * ZRA * ZATL ** 2 / ( ( 1.0 + ZRA ) ** 2 * AM(I,J,K))
C
        ZSPW = ZSTPFR + AMIN1( ZSTPBT , ZSTPLS )
        IF( ZSPW . LE . 0.0 ) GO TO 20
       SPW( L ) = ZSPW
       EEHB1 = EEHB( L + 1 ) - ZSPW * YR(L,J,K) *DX   :(DX IS MESH SIZE IN X)
         IF( EEHB1 . LE . 0.0 ) GO TO 20
       EEHB( L ) = EEHB1
       HEAT( L,J,K ) = ZPE * ( EEHB( L + 1 ) - EEHB( L ) ) /DX
   10 C O N T I N U E
   20 C O N T I N U E
 1000 CONTINUE
```

Fig.6

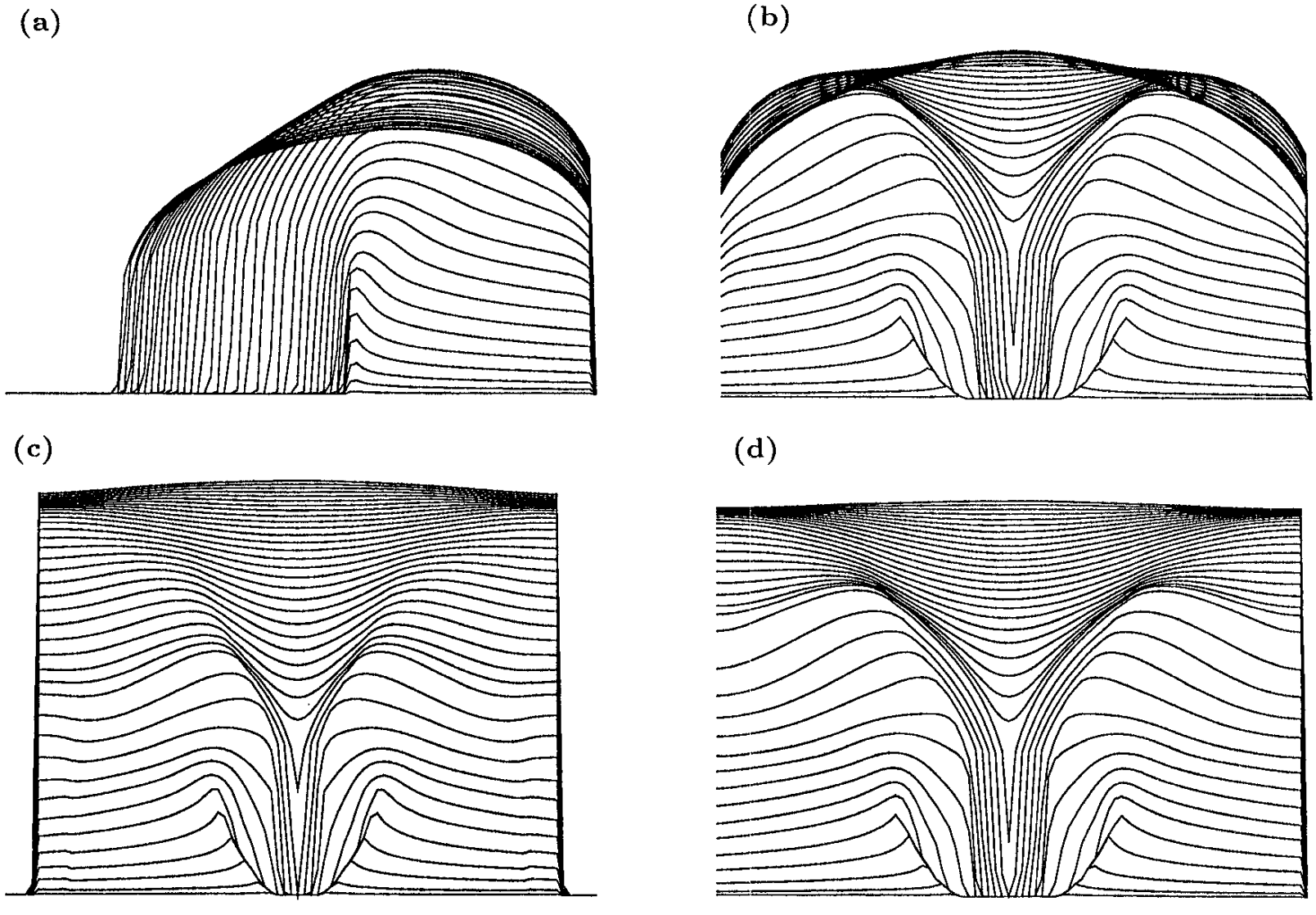

Fig.7

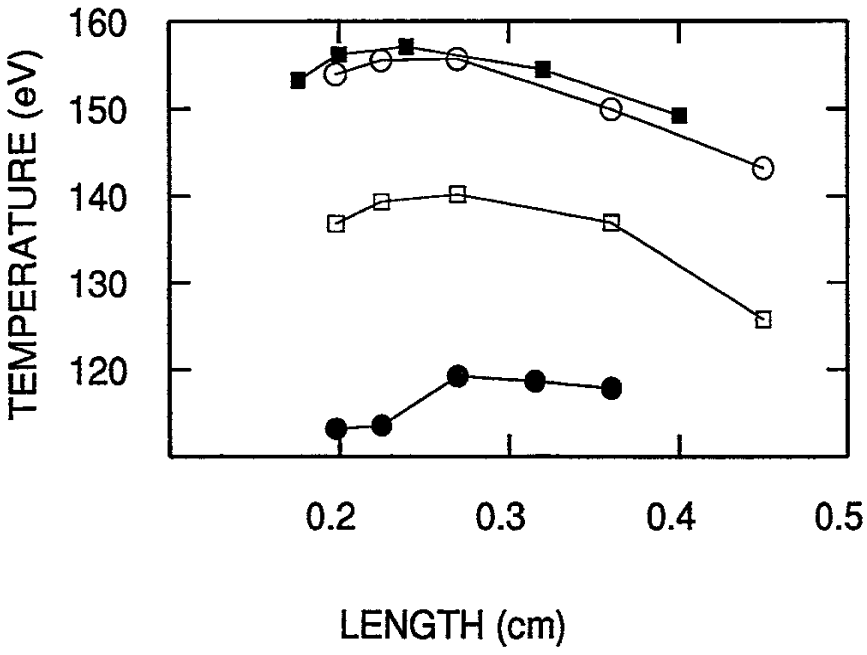

Fig.8

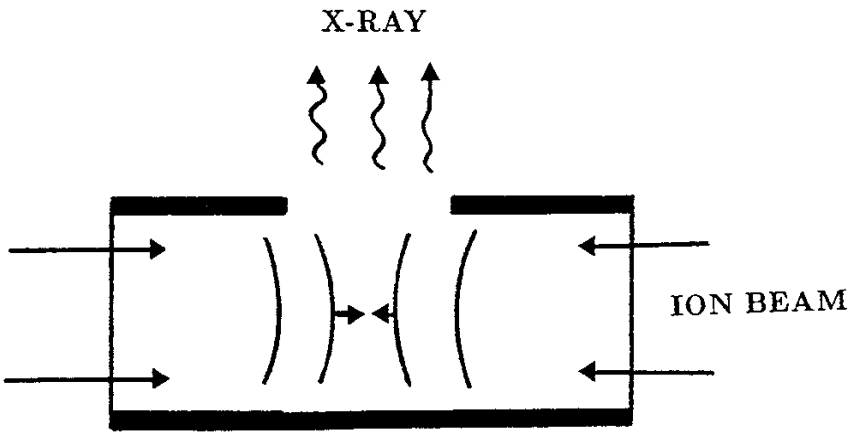

Fig.9

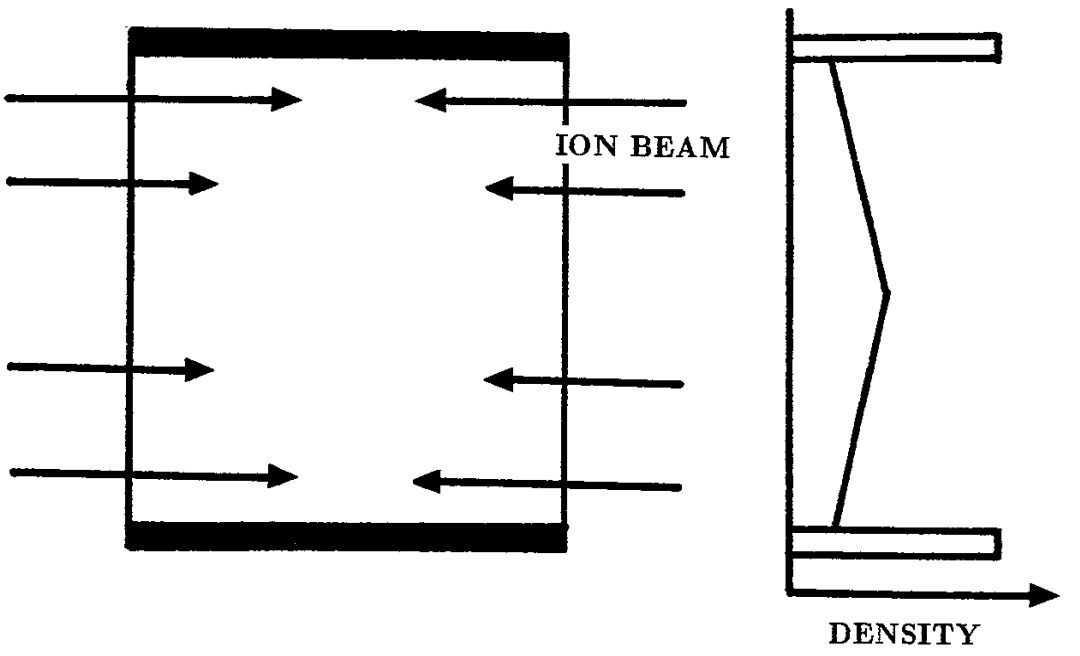

Fig.10

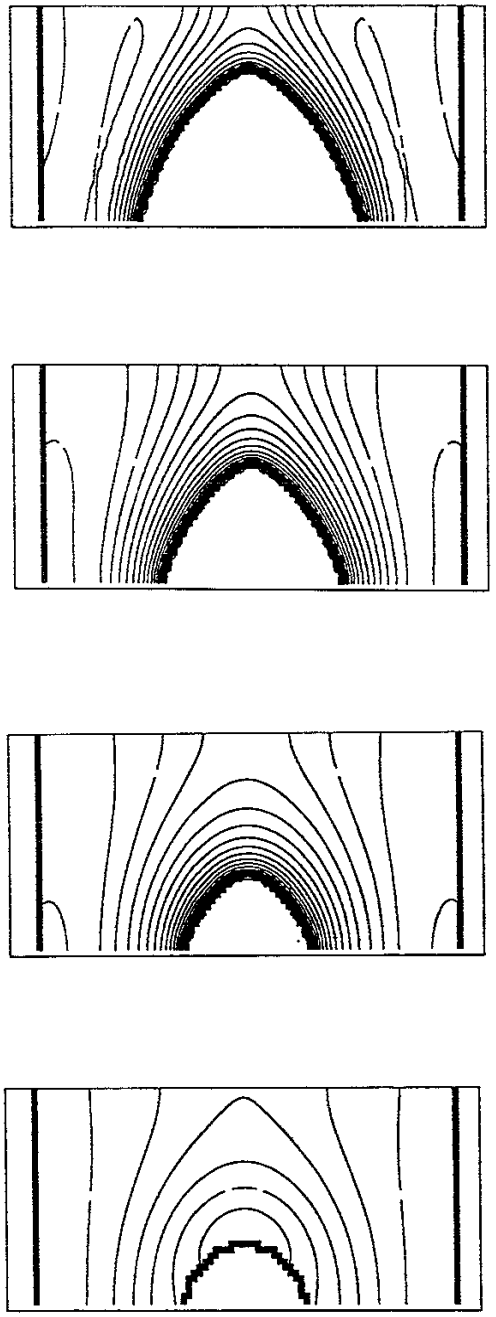

Fig.11

Recent Issues of NIFS Series

NIFS-59 A.Fukuyama, S.-I.Itoh, K.Itoh, K.Hamamatsu, V.S.Chan, S.C.Chiu, R.L.Miller and T.Ohkawa, *Nonresonant Current Drive by RF Helicity Injection*; Oct. 1990

NIFS-60 K.Ida, H.Yamada, H.Iguchi, S.Hidekuma, H.Sanuki, K.Yamazaki and CHS Group, *Electric Field Profile of CHS Heliotron/Torsatron Plasma with Tangential Neutral Beam Injection*; Oct. 1990

NIFS-61 T.Yabe and H.Hoshino, *Two- and Three-Dimensional Behavior of Rayleigh-Taylor and Kelvin-Helmholz Instabilities*; Oct. 1990

NIFS-62 H.B. Stewart, *Application of Fixed Point Theory to Chaotic Attractors of Forced Oscillators;* Nov. 1990

NIFS-63 K.Konn., M.Mituhashi, Yoshi H.Ichikawa,*Soliton on Thin Vortex Filament;* Dec. 1990

NIFS-64 K.Itoh, S.-I.Itoh and A.Fukuyama,*Impact of Improved Confinement on Fusion Research;* Dec. 1990

NIFS -65 A.Fukuyama, S.-I.Itoh and K. Itoh,*A Consistency Analysis on the Tokamak Reactor Plasmas;* Dec. 1990

NIFS-66 K.Itoh, H. Sanuki, S.-I. Itoh and K. Tani,*Effect of Radial Electric Field on α-Particle Loss in Tokamaks;* Dec. 1990

NIFS-67 K.Sato,and F.Miyawaki,*Effects of a Nonuniform Open Magnetic Field on the Plasma Presheath*; Jan.1991

NIFS-68 K.Itoh and S.-I.Itoh,*On Relation between Local Transport Coefficient and Global Confinement Scaling Law;* Jan. 1991

NIFS-69 T.Kato, K.Masai, T.Fujimoto,F.Koike, E.Källne, E.S.Marmar and J.E.Rice,*He-like Spectra Through Charge Exchange Processes in Tokamak Plasmas;* Jan.1991

NIFS-70 K. Ida, H. Yamada, H. Iguchi, K. Itoh and CHS Group, *Observation of Parallel Viscosity in the CHS Heliotron/Torsatron* ; Jan.1991

NIFS-71 H. Kaneko, *Spectral Analysis of the Heliotron Field with the Toroidal Harmonic Function in a Study of the Structure of Built-in Divertor* ; Jan. 1991

NIFS-72 S. -I. Itoh, H. Sanuki and K. Itoh, *Effect of Electric Field Inhomogeneities on Drift Wave Instabilities and Anomalous Transport* ; Jan. 1991

NIFS-73 Y.Nomura, Yoshi.H.Ichikawa and W.Horton, *Stabilities of Regular Motion in the Relativistic Standard Map*; Feb. 1991

NIFS-74 T.Yamagishi, *Electrostatic Drift Mode in Toroidal Plasma with Minority Energetic Particles,* Feb. 1991

NIFS-75 T.Yamagishi, *Effect of Energetic Particle Distribution on Bounce Resonance Excitation of the Ideal Ballooning Mode*, Feb. 1991

NIFS-76 T.Hayashi, A.Tadei, N.Ohyabu and T.Sato, *Suppression of Magnetic Surface Breading by Simple Extra Coils in Finite Beta Equilibrium of Helical System;* Feb. 1991

NIFS-77 N. Ohyabu, *High Temperature Divertor Plasma Operation*; Feb. 1991

NIFS-78 K.Kusano, T. Tamano and T. Sato, *Simulation Study of Toroidal Phase-Locking Mechanism in Reversed-Field Pinch Plasma*; Feb. 1991

NIFS-79 K. Nagasaki, K. Itoh and S. -I. Itoh, *Model of Divertor Biasing and Control of Scrape-off Layer and Divertor Plasmas*; Feb. 1991

NIFS-80 K. Nagasaki and K. Itoh, *Decay Process of a Magnetic Island by Forced Reconnection*; Mar. 1991

NIFS-81 K. Takahata, N. Yanagi, T. Mito, J. Yamamoto, O.Motojima and LHDDesign Group, K. Nakamoto, S. Mizukami, K. Kitamura, Y. Wachi, H. Shinohara, K. Yamamoto, M. Shibui, T. Uchida and K. Nakayama, *Design and Fabrication of Forced-Flow Coils as R&D Program for Large Helical Device*; Mar. 1991

NIFS-82 T. Aoki and T. Yabe, *Multi-dimensional Cubic Interpolation for ICF Hydrodynamics Simulation*; Apr. 1991

NIFS-83 K. Ida, S.-I. Itoh, K. Itoh, S. Hidekuma, Y. Miura, H. Kawashima, M. Mori, T. Matsuda, N. Suzuki, H. Tamai, T.Yamauchi and JFT-2M Group, *Density Peaking in the JFT-2M Tokamak Plasma with Counter Neutral Beam Injection* ; May 1991

NIFS-84 A. Iiyoshi, *Development of the Stellarator/Heliotron Research*; May 1991

NIFS-85 Y. Okabe, M. Sasao, H. Yamaoka, M. Wada and J. Fujita, *Dependence of Au^- Production upon the Target Work Function in a Plasma-Sputter-Type Negative Ion Source;* May 1991

NIFS-86 N. Nakajima and M. Okamoto, *Geometrical Effects of the Magnetic Field on the Neoclassical Flow, Current and Rotation in General Toroidal Systems*; May 1991

NIFS-87 S. -I. Itoh, K. Itoh, A. Fukuyama, Y. Miura and JFT-2M Group, *ELMy-H mode as Limit Cycle and Chaotic Oscillations in Tokamak Plasmas;* May 1991

NIFS-88 N.Matsunami and K.Kitoh, *High Resolution Spectroscopy of H^+ Energy Loss in Thin Carbon Film;* May 1991

NIFS-89 H. Sugama, N. Nakajima and M.Wakatani, *Nonlinear Behavior of Multiple-Helicity Resistive Interchange Modes near Marginally Stable States;* May 1991

NIFS-90 H. Hojo and T.Hatori, *Radial Transport Induced by Rotating RF Fields and Breakdown of Intrinsic Ambipolarity in a Magnetic Mirror*; May 1991

NIFS-91 M. Tanaka, S. Murakami, H. Takamaru and T.Sato, *Macroscale Implicit, Electromagnetic Particle Simulation of Inhomogeneous and Magnetized Plasmas in Multi-Dimensions;* May 1991

NIFS-92 S. - I. Itoh, *H-mode Physics, -Experimental Observations and Model Theories-, Lecture Notes, Spring College on Plasma Physics, May 27 - June 21 1991 at International Centre for Theoretical Physics (IAEA UNESCO) Trieste, Italy ;* Jun. 1991

NIFS-93 Y. Miura, K. Itoh, S. - I. Itoh, T. Takizuka, H. Tamai, T. Matsuda, N. Suzuki, M. Mori, H. Maeda and O. Kardaun, *Geometric Dependence of the Scaling Law on the Energy Confinement Time in H-mode Discharges;* Jun. 1991

NIFS-94 H. Sanuki, K. Itoh, K. Ida and S. - I. Itoh, *On Radial Electric Field Structure in CHS Torsatron / Heliotron;* Jun. 1991

NIFS-95 K. Itoh, H. Sanuki and S. - I. Itoh, *Influence of Fast Ion Loss on Radial Electric Field in Wendelstein VII-A Stellarator;* Jun. 1991

NIFS-96 S. - I. Itoh, K. Itoh, A. Fukuyama, *ELMy-H mode as Limit Cycle and Chaotic Oscillations in Tokamak Plasmas;* Jun. 1991

NIFS-97 K. Itoh, S. - I. Itoh, H. Sanuki, A. Fukuyama, *An H-mode-Like Bifurcation in Core Plasma of Stellarators;* Jun. 1991

NIFS-98 H. Hojo, T. Watanabe, M. Inutake, M. Ichimura and S. Miyoshi, *Axial Pressure Profile Effects on Flute Interchange Stability in the Tandem Mirror GAMMA 10;* Jun. 1991

NIFS-99 A. Usadi, A. Kageyama, K. Watanabe and T. Sato, *A Global Simulation of the Magnetosphere with a Long Tail : Southward and Northward IMF;* Jun. 1991

NIFS-100 H. Hojo, T. Ogawa and M. Kono, *Fluid Description of Ponderomotive Force Compatible with the Kinetic One in a Warm Plasma* ; July 1991

NIFS-101 H. Momota, A. Ishida, Y. Kohzaki, G. H. Miley, S. Ohi, M. Ohnishi K. Yoshikawa, K. Sato, L. C. Steinhauer, Y. Tomita and M. Tuszewski *Conceptual Design of D-^{3}He FRC Reactor "ARTEMIS"* ; July 1991

NIFS-102 N. Nakajima and M. Okamoto, *Rotations of Bulk Ions and Impurities in Non-Axisymmetric Toroidal Systems* ; July 1991

NIFS-103 A. J. Lichtenberg, K. Itoh, S. - I. Itoh and A. Fukuyama, *The Role of Stochasticity in Sawtooth Oscillation* ; Aug. 1991

NIFS-104 K. Yamazaki and T. Amano, *Plasma Transport Simulation Modeling for Helical Confinement Systems;* Aug. 1991

NIFS-105 T. Sato, T. Hayashi, K. Watanabe, R. Horiuchi, M. Tanaka, N. Sawairi and K. Kusano, *Role of Compressibility on Driven Magnetic Reconnection ;* Aug. 1991

NIFS-106 Qian Wen - Jia, Duan Yun - Bo, Wang Rong - Long and H. Narumi, *Electron Impact Excitation of Positive Ions - Partial Wave Approach in Coulomb - Eikonal Approximation* ; Sep. 1991

NIFS-107 S. Murakami and T. Sato, *Macroscale Particle Simulation of Externally Driven Magnetic Reconnection;* Sep. 1991

NIFS-108 Y. Ogawa, T. Amano, N. Nakajima, Y. Ohyabu, K. Yamazaki, S. P. Hirshman, W. I. van Rij and K. C. Shaing, *Neoclassical Transport Analysis in the Banana Regime on Large Helical Device (LHD) with the DKES Code;* Sep. 1991

NIFS-109 Y. Kondoh, *Thought Analysis on Relaxation and General Principle to Find Relaxed State;* Sep. 1991

NIFS-110 H. Yamada, K. Ida, H. Iguchi, K. Hanatani, S. Morita, O. Kaneko, H. C. Howe, S. P. Hirshman, D. K. Lee, H. Arimoto, M. Hosokawa, H. Idei, S. Kubo, K. Matsuoka, K. Nishimura, S. Okamura, Y. Takeiri, Y. Takita and C. Takahashi, *Shafranov Shift in Low-Aspect-Ratio Heliotron / Torsatron CHS* ; Sep 1991

NIFS-111 R. Horiuchi, M. Uchida and T. Sato, *Simulation Study of Stepwise Relaxation in a Spheromak Plasma ;* Oct. 1991

NIFS-112 M. Sasao, Y. Okabe, A. Fujisawa, H. Iguchi, J. Fujita, H. Yamaoka and M. Wada, *Development of Negative Heavy Ion Sources for Plasma Potential Measurement* ; Oct. 1991

NIFS-113 S. Kawata and H. Nakashima, *Tritium Content of a DT Pellet in Inertial Confinement Fusion* ; Oct. 1991

NIFS-114 M. Okamoto, N. Nakajima and H. Sugama, *Plasma Parameter Estimations for the Large Helical Device Based on the Gyro-Reduced Bohm Scaling* ; Oct. 1991

NIFS-115 Y. Okabe, *Study of Au^- Production in a Plasma-Sputter Type Negative Ion Source* ; Oct. 1991

NIFS-116 M. Sakamoto, K. N. Sato, Y. Ogawa, K. Kawahata, S. Hirokura, S. Okajima, K. Adati, Y. Hamada, S. Hidekuma, K. Ida, Y. Kawasumi, M. Kojima, K. Masai, S. Morita, H. Takahashi, Y. Taniguchi, K. Toi and T. Tsuzuki, *Fast Cooling Phenomena with Ice Pellet Injection in the JIPP T-IIU Tokamak;* Oct. 1991

NIFS-117 K. Itoh, H. Sanuki and S. -I. Itoh, *Fast Ion Loss and Radial Electric Field in Wendelstein VII-Λ Stellarator*; Oct. 1991

NIFS-118 Y. Kondoh and Y. Hosaka, *Kernel Optimum Nearly-analytical Discretization (KOND) Method Applied to Parabolic Equations <<KOND-P Scheme>>;* Nov. 1991